Long-term reconstruction of satellite-based precipitation, soil moisture, and snow water equivalent in China

Wencong Yang[1, 2], Hanbo Yang[1,2], Changming Li[1,2], Taihua Wang[1,2], Ziwei Liu[1,2], Qingfang Hu[3], and Dawen Yang[1,2]

[1] Department of Hydraulic Engineering, Tsinghua University, Beijing 100084, China.
[2] State Key Laboratory of Hydro-Science and Engineering, Tsinghua University, Beijing, 100084, China.
[3] State Key Laboratory of Hydrology-Water Resources and Hydraulic Engineering & Science, Nanjing Hydraulic Research Institute, Nanjing 210029, China.

Correspondence to: Hanbo Yang (yanghanbo@tsinghua.edu.cn)

Abstract. A long-term high-resolution national dataset of precipitation (*P*), soil moisture (SM), and snow water equivalent (SWE) is necessary for predicting floods and droughts and assessing the impacts of climate change on streamflow in China. Current long-term daily or sub-daily datasets of *P*, SM, and SWE are limited by a coarse spatial resolution~~,~~ or the lack of local correction~~.~~, Although SM and SWE data derived from hydrological simulations at the national scale have fine spatial resolutions and take advantage of local forcing data, ~~or the~~ hydrological models are not directly calibrated with SM and SWE data~~lack of direct calibration~~. In this study, we produced a daily 0.1° dataset of *P*, SM, and SWE in 1981-2017 across China using global background data and local onsite data as forcing input and satellite-based data as reconstruction benchmarks. ~~Long-term g~~Global 0.1° and local 0.25° *P* data in 1981-2017 are merged to reconstruct the historical *P* ~~from~~ of the ~~short-term~~ 0.1° China Merged Precipitation Analysis (CMPA) available in 2008-2017 using a stacking machine learning model. The reconstructed *P* data are used to drive HBV hydrological model to simulate SM and SWE data in 1981-2017. ~~Long-term~~ The SM ~~data~~ simulation ~~are~~ is ~~reconstructed by the HBV hydrological model with SM~~ calibrated by Soil Moisture Active Passive Level 4 (SMAP-L4) data. ~~Long-term~~ The SWE ~~data~~ simulation ~~are~~ is ~~also reconstructed by the HBV hydrological model with SWE~~ calibrated by the national satellite-based snow depth dataset in China (Che and Dai, 2015) and the Moderate Resolution Imaging Spectroradiometer (MODIS) snow cover data. Cross-validated by the spatial and temporal splitting of CMPA data, ~~For all grids at the national and daily scale,~~ the median Kling-Gupta Efficiency (KGE) of the reconstructed *P* ~~and SM are~~ is 0.68 ~~and 0.61 respectively~~ for all grids at a daily scale. The median KGE of SM in calibration is 0.61 for all grids at the daily scale. For grids in two snow-rich regions ~~at the daily scale~~, the median KGEs of ~~the reconstructed~~ SWE in calibration are 0.55 and -2.41 in the Songhua and Liaohe Basin and the Continental Basin respectively at the daily scale. Generally, the reconstruction dataset performs better in southern and eastern China than in northern and western China for *P* and SM, and performs better in northeast China than other regions for SWE. As the first long-term 0.1° daily dataset of *P*, SM, and SWE that combines information from local observations and satellite-based data benchmarks, this reconstruction product is valuable for future national investigations of hydrological processes.

1 Introduction

A long-term national terrestrial hydrological dataset with high spatial-temporal resolutions can be used in many hydrological applications such as: exploring the controls of rainfall-runoff events (Tarasova et al., 2020; Yang et al., 2020; Stein et al., 2021), predicting floods and droughts (Van Steenbergen and Willems, 2013; Reager et al., 2014; Abelen et al., 2015), and assessing the impacts of climate change on streamflow and floods (Sharma and Wasko, 2018; Blöschl et al., 2019; Li et al, 2019). As key variables in the hydrological cycle, precipitation (P), soil moisture (SM), and snow water equivalent (SWE) generate riverine runoff and determine the wetness states of the basins. Although long-term (at least 30 years) daily P, SM, and SWE can be obtained from many data products in China, these products suffer from a coarse spatial resolution and a lack of local information.

1.1 Limitations of long-term daily or sub-daily precipitation data in China

There are many long-term global precipitation data with a temporal resolution within one day and a spatial resolution within $0.1°$. For example, two popular datasets are the Multi-Source Weighted-Ensemble Precipitation (MSWEP; Beck et al., 2019) and the hourly $0.1°$ dataset ERA5-land (Muñoz-Sabater et al., 2021). MSWEP is a 3-hourly $0.1°$ dataset that begins in 1979 and merges multiple sources including gauge stations, remote sensing observations, and reanalysis data. ERA5-land is an hourly $0.1°$ reanalysis dataset that begins in 1981. Those global datasets have insufficient information ~~of~~ on data from rain gauge stations in China, which leads to limited performance. Two local precipitation datasets are widely used in China. The first one is the China Gauge-based Daily Precipitation Analysis (CGDPA; Shen and Xiong, 2016), which is interpolated from the daily data back to 1960 in approximately 2400 ground stations. The key limitation of CGDPA is its coarse spatial resolution of $0.25°$. The second one is the China Meteorological Forcing Dataset (CMFD; He et al., 2020), which is a 3-hourly $0.1°$ dataset in 1979-2018 using approximately 700 ground stations to correct the Global Land Data Assimilation System (GLDAS; Rodell et al., 2004) and Tropical Rainfall Measuring Mission (TRMM; Huffman et al., 2007) precipitation background data. CMFD does not take full advantage of available precipitation information since better background data (e.g., MSWEP and ERA5-land) and more ground station data are available.

1.2 Limitations of long-term daily or sub-daily soil moisture data in China

Remote sensing and reanalysis data are two common types of global soil moisture data. The European Space Agency's Climate Change Initiative (ESA-CCI; Dorigo et al., 2017) for soil moisture is a global satellite-monitored dataset that begins in 1979. However, ESA-CCI only measures surface soil moisture up to 5 cm depth in a coarse spatial resolution of 25 km. Global reanalysis data, e.g., ERA5-land, can provide soil moisture data in deeper soil layers in a high spatial resolution. However, global reanalysis data miss observational information ~~of~~ on soil moisture, and they simulate soil moisture using global forcing data which lack local corrections. Many hydrologic fluxes and states datasets provide simulated soil moisture data at a national scale. For example, the 3-hourly $0.25°$ dataset based on the VIC model created by Zhang et al. (2014), the daily $0.25°$ dataset

based on the VIC model created by Miao and Wang (2020), and the daily 0.0625° dataset based on the VIC model created by Zhu et al. (2021). However, all these national-scale soil moisture data are simulated by a hydrological model calibrated by

65 only observed streamflow data. Therefore, the lack of direct calibration in ~~observed~~ soil moisture causes uncertain accuracy.

1.3 Limitations of long-term daily or sub-daily snow water equivalent data in China

Similar to soil moisture, remote sensing data and reanalysis data are two common types of global data products for snow water equivalent. GlobSnow (Luojus et al., 2021) is a global daily snow water equivalent dataset that assimilates satellite radiometer data and ground snow depth observations. To promote local applications, Che and Dai (2015) developed a national satellite-

70 based snow depth dataset in China (abbreviated as SD-CN hereafter). Both GlobSnow and SD-CN begin in 1979 with a coarse spatial resolution of 25 km. Global reanalysis data such as ERA5-land, as we stated before, use global forcing input with limited local information. The snow water equivalent data from the national hydrologic fluxes and states datasets (Zhang et al., 2014; Miao and Wang, 2020) have the same problem as soil moisture data, i.e., they are not directly calibrated using any snow ~~observations~~data.

75 **1.4 Objectives**

We aim to use both global and local forcing data as input and satellite-based data as model training or calibration targets to reconstruct historical hydrological variables. This kind of reconstruction is promising in producing long-term high-resolution datasets with the following advantages. First, many satellite-based data have high spatial resolutions. For example, the 0.1° China Merged Precipitation Analysis (CMPA; Shen et al., 2014; Shen et al., 2018) from 2008 for precipitation, the 9 km Soil

80 Moisture Active Passive level 4 data (SMAP-L4; Reichle et al., 2019) from 2015 for root zone soil moisture, and the 500 m Moderate Resolution Imaging Spectroradiometer (MODIS; Hall et al., 2002) from 2000 for snow cover. Second, combining global and local forcing data as input not only increases local reconstruction accuracy, but also produces a physically consistent dataset of the combination of P, SM, and SWE, since they are the hydrological fluxes and states from the same modeling system during the reconstructions.

85 In this study, we produced a daily 0.1° dataset of P, SM, and SWE in 1981-2017 in China. We merged CGDPA and MSWEP to reconstruct the P benchmarked by CMPA using machine learning techniques. We used the reconstructed P to drive a hydrological model to reconstruct SM calibrated by SMAP level 4. ~~For P, we merged CGDPA and MSWEP to reconstruct the~~ ~~P from CMPA using machine learning techniques; for SM, we used the reconstructed P to drive a hydrological model to~~ ~~reconstruct SM from SMAP level 4; for SWE,~~ ~~W~~we also used the reconstructed P to drive a hydrological model calibrated by

90 SD-CN and MODIS snow cover data to reconstruct multiple snow-related variables, e.g., snowfall, snowmelt, and SWE. This is the first long-term (at least 30 years) 0.1° daily dataset of P, SM, and SWE that combines local information and satellite-based data.

2 Data

This study used two categories of data. The first category includes the forcing and auxiliary data, which are the input of the reconstruction methods. The second category includes the validation data of *P*, SM, and SWE, which are ~~the~~reconstruction targets and evaluation benchmarks of the reconstruction methods.

2.1 Forcing and auxiliary data

Information about the forcing data and auxiliary data are listed in Table 1. These data are the input of the reconstruction methods, i.e., machine learning modeling and hydrological modeling. Precipitation data include the China Gauge-based Daily Precipitation Analysis (CGDPA; Shen and Xiong, 2016) and the Multi-Source Weighted-Ensemble Precipitation (MSWEP version 2.2; Beck et al., 2019). The daily 0.25° CGDPA data are produced using a spatial interpolation of observations from approximately 2400 ground rain gauge stations. The 3-hourly 0.1° MSWEP data are produced by optimally merging a range of gauge station, satellite, and reanalysis datasets. In addition to precipitation data, hydrological modeling requires air temperature (*T*) and net radiation data (R_n) as forcing data. Air temperature ~~(*T*)~~ data include the observations from approximately 2400 ground stations provided by the Chinese Meteorological Administration and ERA5-land 2 m temperature (Muñoz-Sabater et al., 2021). Note that the number of available ground stations for *T* is around 800 before 1988. Net radiation ~~(R_n)~~ data are from ERA5-land (Muñoz-Sabater et al., 2021). Elevation (Elev) data are from MERIT-Hydro (Yamazaki et al., 2019). Leaf area index (LAI) data are from the Global Land Surface Satellite (GLASS; Liang et al., 2021) dataset.

Table 1. Sources of forcing and auxiliary data.

Variable	Dataset	Spatial resolution	Temporal resolution	Temporal coverage	Reference
Precipitation	CGDPA	0.25°	daily	1960-2020	Shen and Xiong, 2016
Precipitation	MSWEP	0.1°	3-hourly	1979-2017	Beck et al., 2019
Air temperature	Stations	—	daily	1960-2019	Chinese Meteorological Administration
Air temperature	ERA5-land	0.1°	hourly	1981-now	Muñoz-Sabater et al., 2021
Net radiation	ERA5-land	0.1°	hourly	1981-now	Muñoz-Sabater et al., 2021
Elevation	MERIT-Hydro	90 m	—	—	Yamazaki et al., 2019
Leaf area index	GLASS	0.05°	8-day	1981-2017	Liang et al., 2021

2.2 Validation data

Information about the validation data is listed in Table 2. The validation data are the reconstruction targets of the study, and therefore, they are also used for model training (for precipitation) and calibration (for soil moisture and snow water equivalent).

115 _Details about validation methods are introduced in Section 3._ All following satellite-based data provide direct or indirect measurements of the variables to be reconstructed over a large spatial extent. _P_ data include the China Merged Precipitation Analysis (CMPA; Shen et al., 2014) and its successor, CMPA_1km (Shen et al., 2018). CMPA merge more than 30000 automatic weather stations with the Climate Precipitation Center Morphing (CMORPH; Joyce et al., 2004) product to produce an hourly $0.1°$ dataset from 2008. Starting from 2015, CMPA_1km upgrades CMPA by using more than 40000 automatic

120 weather stations and adding radar _P_ estimations in the merging procedure, which increases the spatial resolution to 1 km. _In this study, CMPA_1km was spatially aggregated into $0.1°$ to extend the time span of the CMPA data. CMPA refers to the combination of CMPA and CMPA_1km in the following part of the paper._ Note that precipitation data during the cold season (from October to April) in northern and western China are mainly derived from remote sensing data since automatic weather stations do not operate under low temperatures (Shen et al., 2014; Shen et al., 2018). SM data are obtained from the Soil

125 Moisture Active Passive mission level 4 (SMAP-L4; Reichle et al., 2019) data. SMAP-L4 assimilates SMAP radiometer brightness temperature into the NASA Catchment land surface model to produce a 3-hourly 9 km volumetric SM dataset in the root zone (0–100 cm). Since there is no direct measurement of SWE, we use snow cover areas and snow depths as surrogates. Snow cover area (SCA) data are obtained from MOD10C1 (Hall and Higgs, 2021b) and MYD10C1 (Hall and Higgs, 2021a), which collect snow extent information by the Moderate-Resolution Imaging Spectroradiometer (MODIS) sensors from Terra

130 and Aqua platforms respectively. Compiled at daily and $0.05°$ scales, MOD10C1 and MYD10C1 provide snow cover percentage and cloud cover percentage at each grid. Snow depth data are obtained from the long-term series of daily snow depth dataset in China (SD-CN; Che and Dai, 2015). The 25 km daily snow depth of SD-CN is derived from the passive microwave brightness temperature from SMMR, SSM/I, and SSMI/S sensors. _Although SD-CN is long enough for many hydrological studies, it is limited by a coarse spatial resolution._

135

Table 2. Sources of validation data.

Variable	Dataset	Spatial resolution	Temporal resolution	Temporal coverage	Reference
Precipitation	CMPA	$0.1°$	hourly	2008-2014	Shen et al., 2014
Precipitation	CMPA_1km	1 km	hourly	2015-2017	Shen et al., 2018
Soil moisture	SMAP-L4	9 km	3-hourly	2015-now	Reichle et al., 2019
Snow cover area	MOD10C1	$0.05°$	daily	2000-now	Hall and Higgs, 2021b
Snow cover area	MYD10C1	$0.05°$	daily	2000-now	Hall and Higgs, 2021a
Snow depth	SD-CN	25 km	daily	1979-2019	Che and Dai, 2015

3 Methods

The workflow of the study is presented in Fig. 1. Firstly, we reconstruct the precipitation data, and then, we use the reconstructed precipitation as forcing input to reconstruct soil moisture and snow water equivalent.
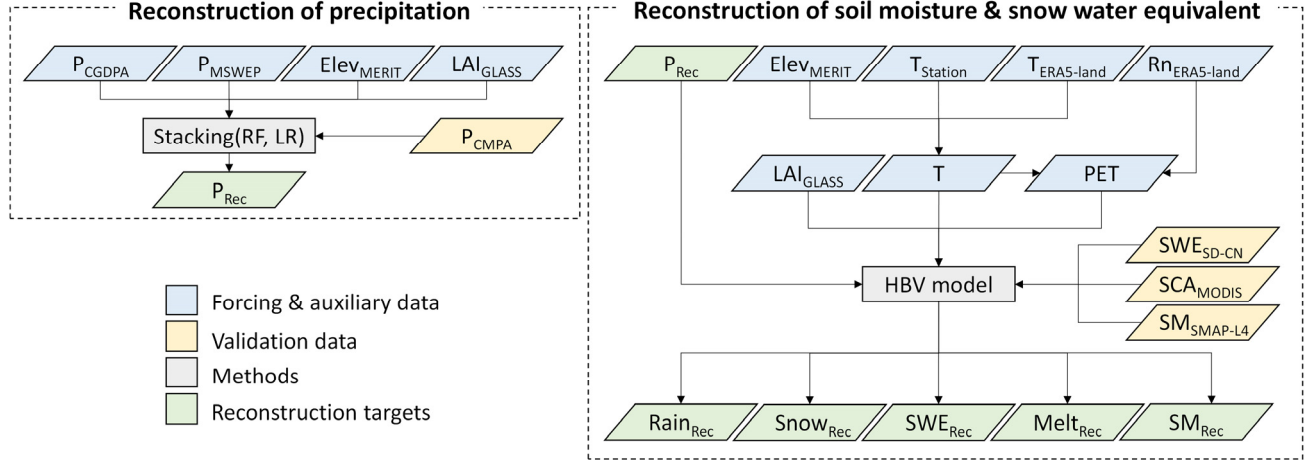
Figure 1. Workflow of the study. P: precipitation, Elev: elevation, LAI: leaf area index, T: air temperature, Rn: net radiation, PET: potential evaporation, SWE: snow water equivalent, SCA: snow cover area, SM: soil moisture, Rain: liquid rainfall, Snow: snowfall, Melt: snowmelt, RF: random forest, LR: linear regression.

3.1 Reconstruction of precipitation

We applied machine learning to predict CMPA precipitation grid by grid using grid coordinates, P from CGDPA and MSWEP, Elev, and LAI as input. All data were pre-processed to be daily and 0.1°. under the WGS 84 latitude/longitude coordinate system (EPSG:4326). MSWEP P and CMPA P were aggregated to be daily. GLASS LAI was set to be the same within the 8 days of an 8-day composite. The CMPA_1km P and MERIT-Hydro Elev data were spatially aggregated into 0.1°. The CGDPA P data were resampled into 0.1° using bilinear interpolation. The difference between the ground-truth 0.1° P and the resampled 0.1° P from CGDPA is spatially correlated with the sub-grid distribution of Elev and LAI in a 0.25° grid. Therefore, we created two new input features, $Elev_{diff}$ and LAI_{diff}, to account for the differences between the true 0.1° value and the value resampled from a 0.25° resolution for Elev and LAI. Specifically, Elev and LAI were aggregated into 0.25°, resampled into 0.1° using bilinear interpolation, and then subtracted by the original 0.1° layer.

The training strategy is presented in Fig. 2. We divided the model training into two parts, a binary classification problem that predicted whether the grid was rainy ($P>0$ mm) and a regression problem which predicted the value of P in rainy grids. We proposed a tile-by-tile training strategy that fit a machine learning model with all samples of one hundred 0.1° grids in a 1° tile. To be specific, although the targeted P_{CMPA} in a 0.1° grid was predicted by grid coordinates, P_{CGDPA}, P_{MSWEP}, Elev, $Elev_{diff}$,

LAI, and LAI$_{diff}$ in the same grid, all grids in the same 1° tile shared a common prediction model. This tile-by-tile training strategy increased the size of samples and made use of the spatial information of Elev and LAI. Since the CMPA data were not reliable during the cold season in northern and western China because of lacking ground-based observations, we discarded training samples from October to April in two regions (Shen et al., 2018): (1) latitude>40° N; (2) 40° N>latitude>27° N and longitude<100° E.
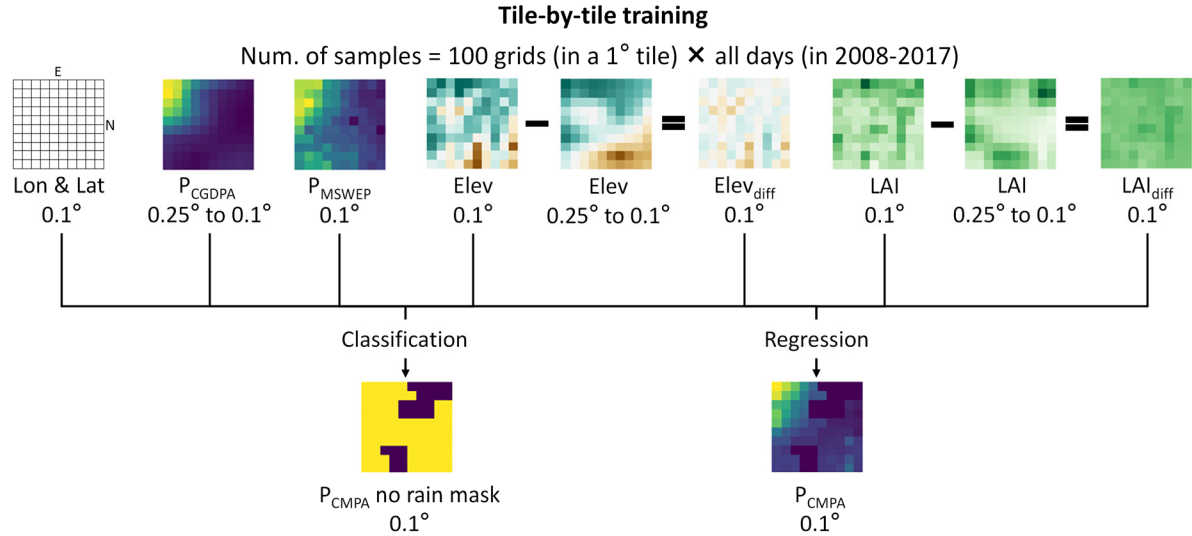
Figure 2. Model training strategies of precipitation reconstruction. P: precipitation, Elev: elevation, LAI: leaf area index.

The machine learning model for the rain/no rain classification is the random forest (Breiman, 2001). The model for the P regression is a neural network (Foresee and Hagan, 1997) that stacks a linear regression model and a random forest model, as shown in Fig. 3. Stacking (Wolpert, 1992) is a model ensemble method that optimally combines multiple base machine learning models for predictions. In the stacking process, all base models are first trained to get out-of-bag predictions in the cross-validation, and then a stacking model is trained using the out-of-bag predictions of the base models as input. The random forest model can deal with non-linear relationships and complex interactions among input features. The linear model can extrapolate the predictions that are out of the range of training samples. A stacking model leveraged the advantages of these two base models. We chose 5-fold cross-validation for hyper-parameter tuning and performance evaluation in both the classification and regression problems. All folds were created by the spatial and temporal mixed splitting of the data samples. Specifically, we put the data of one hundred 0.1° grids in a 1° tile on all days together to form a training dataset and then split it into 5 folds randomly. Each sample corresponded to the data of one 0.1° grid on one day. After the model training, we used the data of P_{CGDPA} and P_{MSWEP} in 1981-2017 combined with grid coordinates, Elev, Elev$_{diff}$, LAI, and LAI$_{diff}$ to predict P_{CMPA} in the same

period, which produced a consistent long-term reconstructed dataset P_{Rec}, as shown in Fig. 1. Note that we only predicted P values on rainy days according to the classification model during the reconstruction.

185
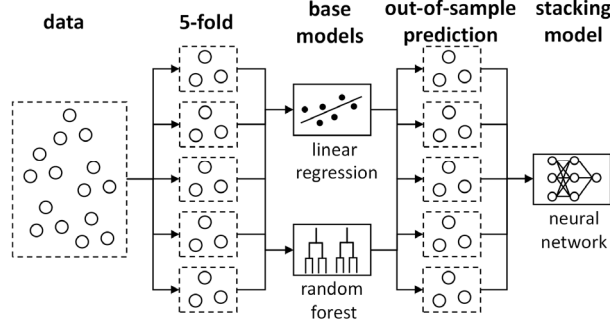
Figure 3. Illustration of a stacking machine learning model for precipitation reconstruction.

Validation metrics include two classification metrics, i.e., probability of detection (POD) and false alarm rate (FAR), and two regression metrics, i.e., Kling-Gupta Efficiency (KGE) and normalized root mean square error (NRMSE). Equations of the

190   metrics are listed in Eq. 1 to 4:

$$\text{POD} = \frac{n_{11}}{n_{11}+n_{01}},\tag{1}$$

$$\text{FAR} = \frac{n_{10}}{n_{11}+n_{10}},\tag{2}$$

$$\text{KGE} = 1 - \sqrt{(r-1)^2 + \left(\frac{\mu_S}{\mu_O}-1\right)^2 + \left(\frac{\sigma_S/\mu_S}{\sigma_O/\mu_O}-1\right)^2},\tag{3}$$

$$\text{NRMSE} = \frac{\sqrt{\frac{1}{n}\sum_{i=1}^{n}(S_i-O_i)^2}}{\sigma_O},\tag{4}$$

195   where n_{11} is the number of actual rainy days that are predicted to be rainy, n_{01} is the number of actual rainy days that are predicted to have no rain, n_{10} is the opposite of n_{01}, r is the correlation between predicted and ~~observed~~ target P, μ_O and μ_S are the mean values of target ~~observed~~ and predicted P respectively, σ_O and σ_S are the standard deviations of target ~~observed~~ and predicted P respectively, S_i is the predicted value of P on the ith rainy day, O_i is the target ~~observed~~ value of P on the ith rainy day. The perfect values are 1 for POD and KGE and 0 for FAR and NRMSE. Note that the predictions are validated in

200   5-fold cross-validation of the model. For grids in northern (latitude>40° N) and western (40° N>latitude>27° N and longitude<100° E) China, only predictions in May-September are validated.

3.2 Reconstruction of soil moisture and snow water equivalent

We used the modified HBV hydrological model (Bergström, 1992; Parajka et al., 2007) calibrated by satellite-based ~~observations~~ data grid by grid to reconstruct SWE and SM. The HBV model has low computational complexity and general applicability in various climate conditions (Beck et al., 2020; Seibert and Bergström, 2022) and show high capability in simulating soil moisture in various regions of the world (Beck et al., 2021). Note that we added a canopy interception module (Mao and Liu, 2019) to the traditional HBV model, as presented in Fig. 4. The HBV model is calibrated at a 0.1° resolution under the WGS 84 latitude/longitude coordinate system (EPSG:4326). The forcing input of the model includes P, T, and potential evaporation (PET). The reconstructed P was regarded as the precipitation input. The 0.1° T was created by the interpolation of observations from ground stations using Co-Kriging (Myers, 1982) with Elev and the daily-aggregated ERA5-land T as covariates. PET was calculated using Priestley-Taylor equation (Priestley and Taylor, 1972) with interpolated T and daily-aggregated ERA5-land Rn.

The calibration targets ~~were~~ SCA, SWE, and SM~~, which should be~~ were pre-processed from the raw ~~observational~~ data ~~before calibration~~ in Table 2. The 0.05° SCA data from MOD10C1 or MYD10C1 were first aggregated to be 0.1°. Then, for each grid, we extracted all days in November-April when the cloud cover percentages were smaller than 40% and calculated the percentage of snow extent in the no cloud fraction of the grid to get the final SCA. The calibration of SCA was converted to a binary classification problem where the ~~observed~~ SCA from MOD10C1 or MYD10C1 was set to ~~be~~ 1 if SCA>10% ~~and~~ otherwise 0 ~~vice versa~~. In the HBV model, SCA was calculated by the binarization of SWE, which meant SCA=1 if SWE exceeded a snowpack threshold T_{cover} otherwise ~~and~~ SCA=0 ~~vice versa~~. For SWE, we first resampled the 25 km snow depth from SD-CN into 0.1° using bilinear interpolation. Then, the ~~observed~~ SWE was calculated by multiplying snow depth and snow density. We used a fixed value of snow density at a national scale, 0.18 g cm^{-3}, which was reasonable for a range part of China (Yang et al., 2019; Gao et al., 2020; Yang et al., 2020). For SM, the 1 m root zone SM from SMAP-L4 was resampled from 9 km to 0.1° using bilinear interpolation and aggregated from ~~3 hourly~~ 3 hours to 1 ~~daily~~ day.
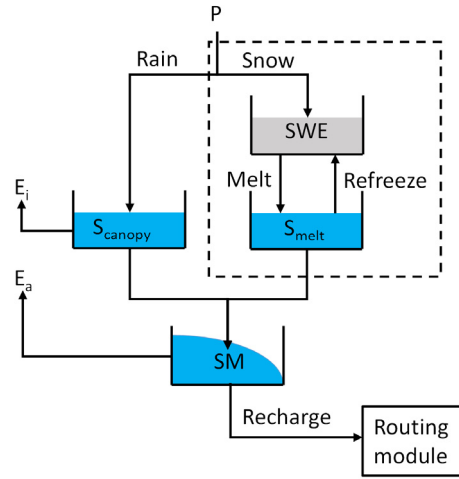
Figure 4. Illustration of the HBV model used for the reconstruction of soil moisture and snow water equivalent. The dashed box illustrates the snow module.

230 For each grid, we first calibrated the parameters of the snow module and then calibrated the soil water module with the optimal snow module parameters. This two-step calibration strategy alleviated parameter equifinality since two modules were calibrated separately. The snow module was only calibrated in grids where at least 5% days with $T<0°C$. All parameters to be calibrated are presented in Table 3. After calibration, we used the historical P_{Rec}, PET, T, and LAI to drive the HBV model to simulate long-term rainfall ($Rain_{Rec}$), snowfall ($Snow_{Rec}$), snow water equivalent (SWE_{Rec}), snowmelt ($Melt_{Rec}$), and soil
235 moisture (SM_{Rec}), as shown in Fig. 1.

Table 3. Parameters of the HBV model and their ranges for model calibration.

Module	Parameters	Description	Range
Snow	TP	Critical temperature for rainfall and snowfall (°C)	[-3, 3]
	TM	Critical temperature for snowmelt and refreezing (°C)	[-3, 3]
	SCF	Correction factor for snowfall	[0.9, 1.5]
	CFX	Degree-day factor (mm °C^{-1} d^{-1})	[0.5, 10]
	CWH	Fraction of snowpack that can hold melt water	[0, 0.2]
	T_{cover}	Snowpack threshold for 10% snow cover areas (mm)	[2, 10]
Soil	m_c	Coefficient for interception storage capacity per unit LAI (mm)	[0.1, 0.5]
	FC	Soil storage capacity (mm)	[50, 800]
	beta	Shape coefficient in runoff generation curve	[0.1, 6]
	LP	Soil moisture above which soil evaporation reaches potential evaporation	[0.2, 1]

The Validation metric for *SCA* is balanced accuracy (BACC):

$$\text{BACC} = \left(\frac{n_{11}}{n_{11}+n_{01}} + \frac{n_{00}}{n_{00}+n_{10}}\right)/2 \, , \tag{5}$$

Where n_{11} is the number of snow cover days that are predicted to have snow cover, n_{00} is the number of no snow cover days that are predicted to have no snow cover, n_{01} is the number of snow cover days that are predicted to have no snow cover, n_{10} is the opposite of n_{01}.

The validation metric for SWE and SM is KGE in Eq. 3, where r is the correlation between predicted and ~~observed~~ target SWE or SM, σ_O and σ_S are the standard deviations of target ~~observed~~ and predicted SWE or SM respectively, μ_O and μ_S are the mean values of target ~~observed~~ and predicted SWE or SM respectively. During the calibration, the optimization target of the snow module was 1-1/4×BACC-3/4×KGE, which optimized the simulation performances of SCA and SWE at the same time. With small numbers of model parameters, the parsimonious snow and soil water modules were unlikely to overfit the target ~~observed~~ data. Therefore, we validated the performance of the reconstruction using the performance of the calibration directly.

4 Results and discussion

4.1 Validation of precipitation

Table 4 summarises the performance of different P datasets in all grids benchmarked by P_{CMPA}. For rain/no rain classification, the reconstructed P (P_{Rec}) achieves a balance of the POD and FAR. The median POD of P_{Rec} is 0.87, which is slightly worse than P_{CGDPA} (POD=0.92) and far better than P_{MSWEP} (POD=0.74). The median FAR of P_{Rec} is 0.19, which is better than P_{CGDPA} (FAR=0.23) but slightly worse than P_{MSWEP} (FAR=0.18). Since the 0.1° P_{CGDPA} is resampled from the 0.25° dataset, it certainly overestimates the probability of rain and has a high POD and FAR at the same time naturally. On the opposite, with the finer spatial information from satellite data, P_{MSWEP} is skilled in detecting no-rain days and thus, it tends to have better FAR performance. In summary, P_{Rec} improves the FAR of P_{CGDPA} without scarifying too many POD. For P regression, P_{Rec} outperforms P_{CGDPA} and P_{MSWEP} significantly. The median KGEs of P_{Rec}, P_{CGDPA}, and P_{MSWEP} are 0.68, 0.51, and 0.53 respectively and the median NRMSEs of P_{Rec}, P_{CGDPA}, and P_{MSWEP} are 0.63, 0.91, and 0.82 respectively.

Table 4. Validation of the reconstructed precipitation in all grids at the national scale. The benchmark dataset is CMPA. POD: probability of detection, FAR: false alarm rate, KGE: Kling-Gupta efficiency, NRMSE: normalized root mean squared error. In northern (latitude>40° N) and western (40° N>latitude>27° N and longitude<100° E) China, only data in May-September are used for validation.

Metric	Percentile	CGDPA	MSWEP	Reconstruction
	Min.	0.18	0.03	0
POD	1st quartile	0.85	0.62	0.81
	Median	0.92	0.74	0.87

	3rd quartile	0.95	0.82	0.91
	Max.	1	0.96	1
FAR	Min.	0.01	0.01	0.01
	1st quartile	0.17	0.12	0.14
	Median	0.23	0.18	0.19
	3rd quartile	0.3	0.24	0.25
	Max.	0.94	0.95	1
KGE	Min.	<-10	<-10	<-10
	1st quartile	0.11	0.17	0.44
	Median	0.51	0.53	0.68
	3rd quartile	0.74	0.71	0.83
	Max.	0.96	0.93	0.97
NRMSE	Min.	0.22	0.32	0.16
	1st quartile	0.6	0.67	0.48
	Median	0.91	0.82	0.63
	3rd quartile	1.22	1.02	0.8
	Max.	>10	>10	>10

Table 5 presents the median values of all metrics for P_{Rec} in nine major basins of China. Figure 5 presents the spatial distribution of validation metrics for P_{Rec} and the metric differences between P_{Rec} and P_{CGDPA} as well as P_{Rec} and P_{MSWEP}. For rain/no rain

270 classification, P_{Rec} performs well since the median POD>0.83 and FAR<0.22 for all major basins except for the Southwest Basin, according to Table 5. According to Fig. 5 (a) and (d), the best performance occurs in the driest part of the Continental Basin where rain is rare, and the worst performance occurs in the plateau such as the upper stream areas of the Yangtze River Basin and the Southwest Basin. The balance of POD and FAR can be seen in Fig. 5 (b), (c), (e), and (f), where P_{Rec} trades POD for FAR compared with P_{CGDPA} and trades FAR for POD compared with P_{MSWEP}. For P regression, in addition to the

275 Continental Basin and the upper stream of the Southwest Basin where the coverage of ground stations is low (Shen et al., 2014; Shen et al., 2018), all other major basins have median KGEs over 0.76 and NRMSEs under 0.55, which indicates good performance, according to Table 5. According to Fig. 5 (g) and (j), with KGE>0.8 and NRMSE<0.5 in a majority of grids, P_{Rec} is very accurate in a large part of the eastern region, probably because of the dense distribution of ground stations for CGDPA (Shen and Xiong, 2016). According to Fig 5 (h), (i), (k), and (l), P_{Rec} outperforms P_{CGDPA} and P_{MSWEP} almost in the

280 whole country. P_{Rec} improves P_{CGDPA} and P_{MSWEP} the most in the Continental Basin and the upper stream of the Southwest Basin where the distribution of ground stations is sparse, even though the performance of P_{Rec} is still limited in this area.

Table 5. Validation of the reconstructed precipitation in nine major basins of China. The benchmark dataset is CMPA. POD: probability of detection, FAR: false alarm rate, KGE: Kling-Gupta efficiency, NRMSE: normalized root mean squared error. In northern (latitude>40° N) and western (40° N>latitude>27° N and longitude<100° E) China, only data in May-September are used for validation.

No.	Basin	Median POD	Median FAR	Median KGE	Median NRMSE
1	Continental Basin	0.9	0.17	0.43	0.8
2	Yangtze River Basin	0.83	0.21	0.82	0.48
3	Songhua and Liaohe River Basin	0.84	0.22	0.76	0.55
4	Southwest Basin	0.75	0.27	0.43	0.8
5	Yellow River Basin	0.89	0.17	0.81	0.5
6	Huaihe River Basin	0.9	0.14	0.88	0.39
7	Haihe River Basin	0.92	0.13	0.86	0.42
8	Southeast Basin	0.86	0.17	0.88	0.39
9	Pearl River Basin	0.85	0.17	0.82	0.49
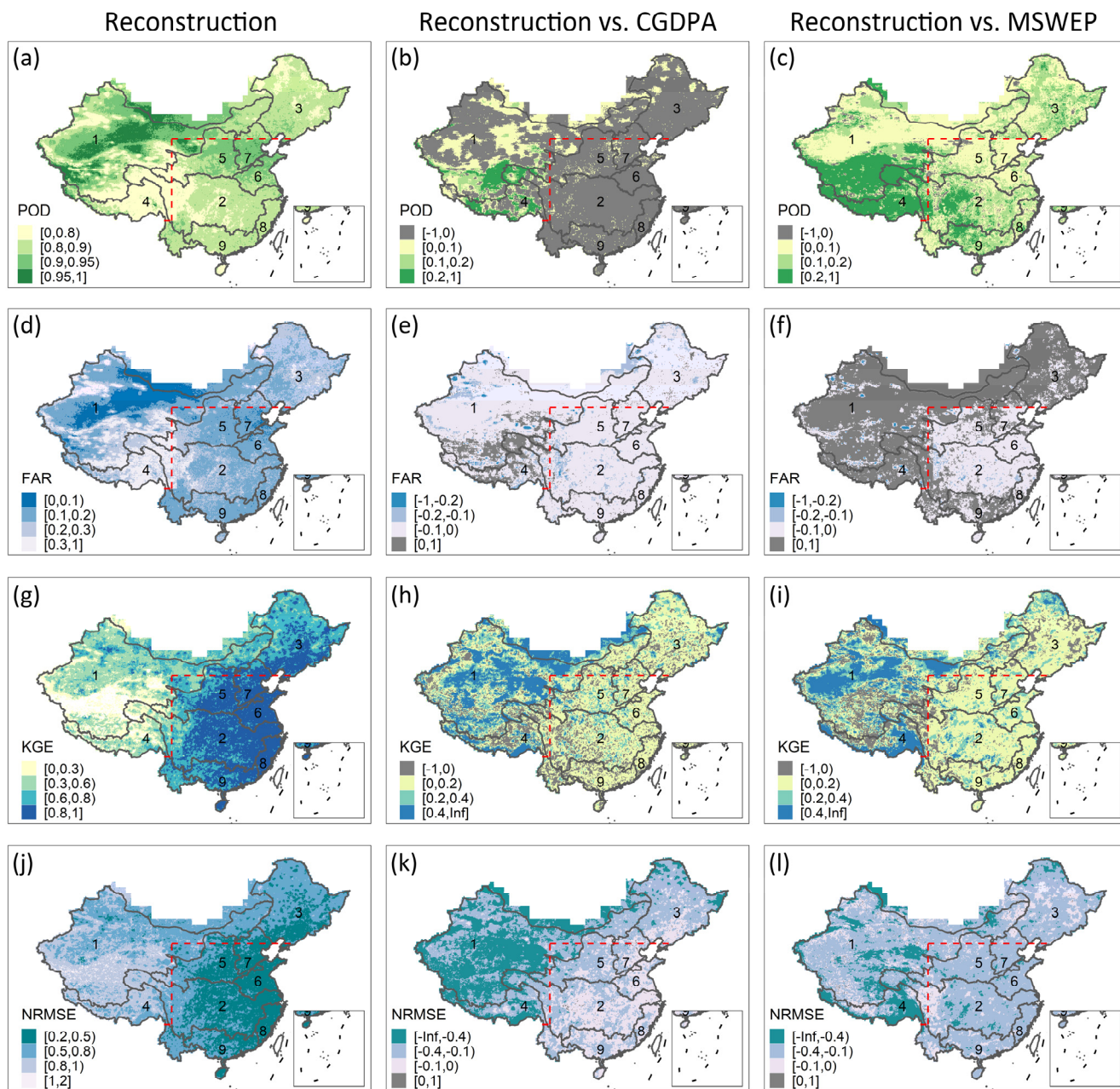
Figure 5. Spatial validation of the reconstructed precipitation. The benchmark dataset is CMPA. POD: probability of detection, FAR: false alarm rate, KGE: Kling-Gupta efficiency, NRMSE: normalized root mean squared error. The second and third columns are the differences of validated metrics between the reconstructed dataset and the CGDPA and MSWEP datasets. The boundary lines delineate nine major river basins of China: 1. the Continental Basin, 2. the Yangtze River Basin, 3. the Songhua and Liaohe River Basin, 4. the Southwest Basin, 5. the Yellow River Basin, 6. the Huaihe River Basin, 7. the Haihe River Basin, 8. the Southeast Basin, 9. the Pearl River Basin. In northern (latitude>40° N) and western (40° N>latitude>27° N and longitude<100° E) China above the dashed lines, only data in May-September are validated.

Figure 6 presents the spatial distribution of annual average *P* and the time series of monthly *P* for P_{CMPA} and P_{Rec}. P_{Rec} matches P_{CMPA} well both spatially and temporally for nine major basins at a large temporal scale. According to Fig. 6 (a), P_{Rec} does not smooth the spatial distribution of *P*, which indicates that the tile-by-tile training strategy learns the local variations of *P* within the tile. Except for the Continental Basin and the Songhua and Liaohe River Basin where the cold season precipitation data are not reliable for CMPA, all other basins have KGE values larger than 0.91 for monthly time series, according to Fig. 6 (b).
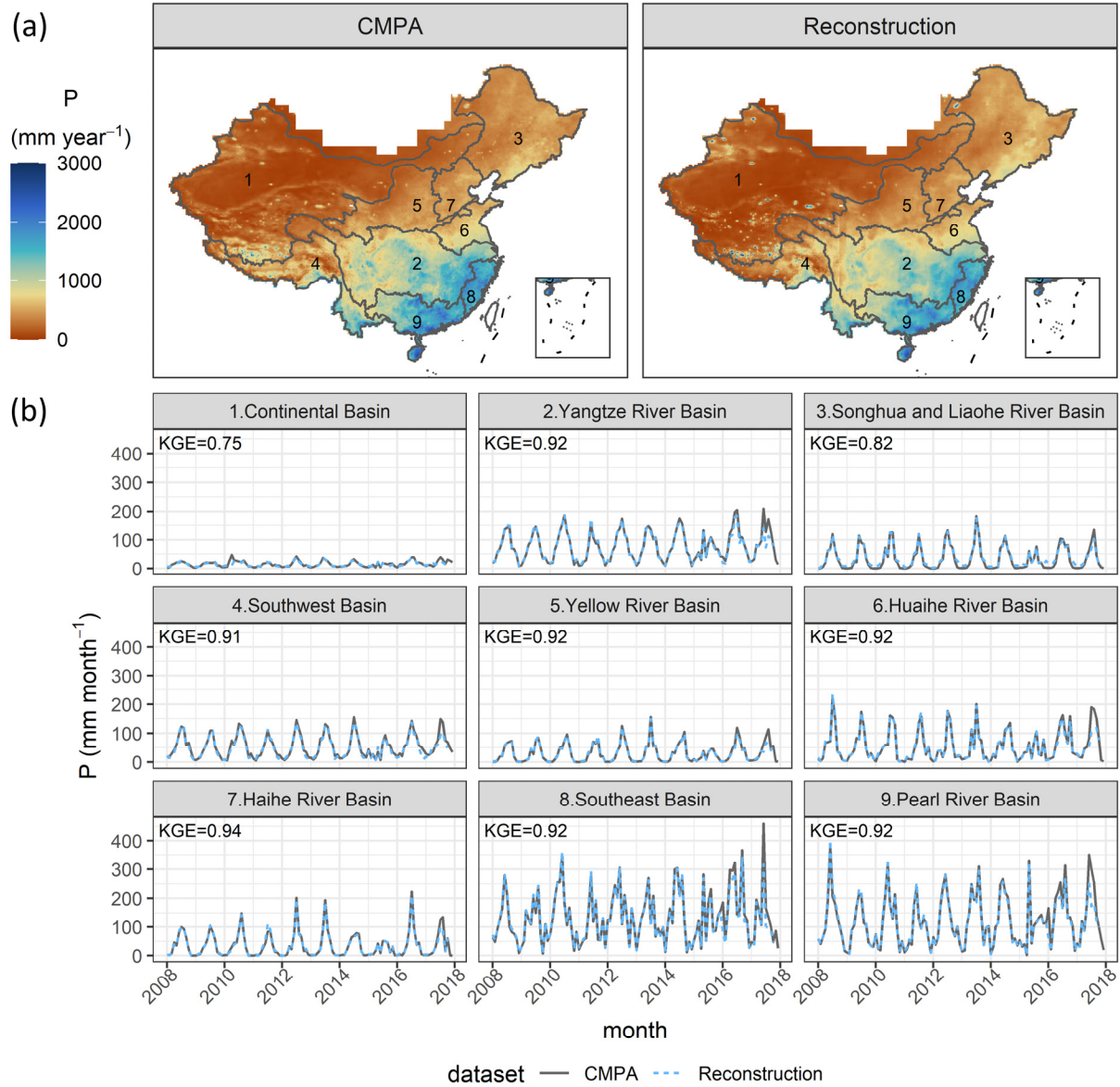
 Figure 6. (a) Map of the annual average precipitation (P) of CMPA and reconstruction in 2008-2017. (b) Time series of the monthly P of CMPA and reconstruction for nine major river basins in 2008-2017. Note that CMPA has missing values in 2015, we only choose the days when CMPA has available data in the temporal aggregation for both CMPA and reconstruction. Here the reconstructed P data are out-of-bag predictions in the cross-validation.

4.2 Validation of soil moisture and snow water equivalent

Table 6 summarises the performance of reconstructed SWE_{Rec}, SCA_{Rec}, and SM_{Rec} in all grids. The snow module of the HBV model performs poorly with the median KGE=-0.31 for SWE_{Rec} at a national scale. While the snow module has certain skills in simulating snow cover with the median BACC=0.65 for SCA_{Rec}. The soil water module of the HBV model performs well with the median KGE=0.61 for SM_{Rec}.

Table 7 presents the median values of all metrics for SWE_{Rec}, SCA_{Rec}, and SM_{Rec} in nine major basins of China. Figure 7 presents the spatial distribution of validation metrics for SWE_{Rec}, SCA_{Rec}, and SM_{Rec}. The performance of snow reconstruction varies spatially. There are three major snow cover areas in China: northeast China, northern Xinjiang, and the Tibetan Plateau. According to Fig. 7 (a) and (b), SWE_{Rec} and SCA_{Rec} perform well in both northeast China and northern Xinjiang with $KGE_{SWE}>0.7$ and $BACC_{SCA}>0.8$ in many grids. While SWE_{Rec} and SCA_{Rec} perform poorly with $KGE_{SWE}<0$ and $BACC_{SCA}<0.5$ in a large part of the Tibetan Plateau, where snow-driven hydrological processes are complex (Gao et al., 2020). According to Table 7, SWE_{Rec} and SCA_{Rec} perform the best in the Songhua and Liaohe River Basin (i.e., northeast China) with $KGE_{SWE}=0.55$ and $BACC_{SCA}=0.87$, where ~~and~~ snowmelt contributes a considerable amount of water to runoff and floods (Qi et al., 2021). The performance of soil moisture reconstruction also varies spatially. According to Fig. 7 (c), SM_{Rec} performs well in a large part of southern China. However, in the Continental Basin where the climate is dryer and the topography is more complex, SM_{Rec} performs relatively poorly with median $KGE_{SM}=0.3$. Generally, SM_{Rec} performs better in southern basins, e.g., the Yangtze River Basin, the Huaihe River Basin, the Southeast Basin, and the Pearl River Basin, where the values of median KGE_{SM} are at least 0.76, according to Table 7. Note that the accuracy of SWE_{Rec}, SCA_{Rec}, and SM_{Rec} in different areas may depend on the quality of the benchmark datasets and the ability of the HBV model to represent local hydrological processes.

Table 6. Validation of the reconstructed snow water equivalent (SWE), snow cover area (SCA), and soil moisture (SM) in all grids at the national scale. The benchmark datasets are SD-CN for SWE, MOD10C1/MYD10C1 for SCA, and SMAP-L4 for SM. KGE: Kling-Gupta efficiency, BACC: balanced accuracy.

Percentile	KGE_{SWE}	$BACC_{SCA}$	KGE_{SM}
Min.	<-10	0.22	-1.83
1st quartile	-4.76	0.54	0.33
Median	-0.31	0.65	0.61
3rd quartile	0.36	0.82	0.80
Max.	0.90	1.00	0.99

Table 7. Validation of the reconstructed snow water equivalent (SWE), snow cover area (SCA) in nine major basins of China. The benchmark datasets are SD-CN for SWE, MOD10C1/MYD10C1 for SCA, and SMAP-L4 for SM. KGE: Kling-Gupta efficiency, BACC: balanced accuracy.

No.	Basin	Median KGE$_{SWE}$	Median BACC$_{SCA}$	Median KGE$_{SM}$
1	Continental Basin	-2.41	0.64	0.3
2	Yangtze River Basin	-0.57	0.53	0.79
3	Songhua and Liaohe River Basin	0.55	0.87	0.7
4	Southwest Basin	-0.85	0.6	0.59
5	Yellow River Basin	0.16	0.57	0.65
6	Huaihe River Basin	0.3	0.54	0.76
7	Haihe River Basin	0.37	0.64	0.73
8	Southeast Basin	—	—	0.8
9	Pearl River Basin	—	—	0.88
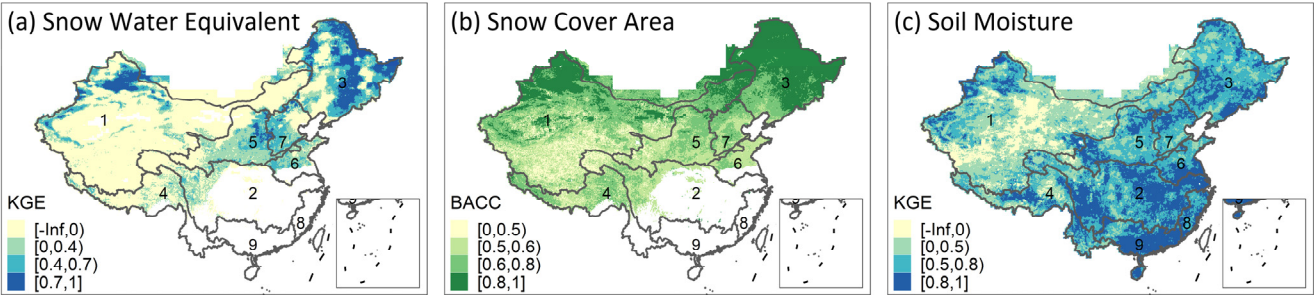
Figure 7. Spatial validation of the reconstructed snow water equivalent (SWE), snow cover area (SCA), and soil moisture (SM). The benchmark datasets are SD-CN for SWE, MOD10C1/MYD10C1 for SCA, and SMAP-L4 for SM. KGE: Kling-Gupta efficiency, BACC: balanced accuracy. The boundary lines delineate nine major river basins of China: 1. the Continental Basin, 2. the Yangtze River Basin, 3. the Songhua and Liaohe River Basin, 4. the Southwest Basin, 5. the Yellow River Basin, 6. the Huaihe River Basin, 7. the Haihe River Basin, 8. the Southeast Basin, 9. the Pearl River Basin.

Figure 8 presents the spatial distribution of daily average SWE and the time series of daily average SWE for SWE$_{SD-CN}$ and SWE$_{Rec}$ in each month. Fig. 8 (a) shows that SWE$_{Rec}$ successfully detects areas with large SWE. Fig. 8 (b) shows that, although SWE$_{Rec}$ captures the temporal variations of SWE in all basins, it overestimates the magnitudes of SWE in the Continental Basin, the Yangtze River Basin, the Southwest Basin, and the Yellow River Basin. In the Songhua and Liaohe River Basin with KGE=0.68 and the Haihe River Basin with KGE=0.46, SWE$_{Rec}$ can accurately capture both the temporal variations and the magnitudes of SWE. The magnitudes of SWE are difficult to simulate for three reasons. First, SWE$_{SD-CN}$ is ~~not the actual observed SWE but~~ an estimation of SWE from the multiplication of snow depth and a fixed snow density; second, the original spatial resolution of SWE$_{SD-CN}$ is 25km, which may be too coarse to represent snow distribution, especially in mountain regions;

third, the new reconstructed precipitation dataset may not capture snowfall well. Figure 9 presents the spatial distribution of daily average SM and the time series of daily average SM for $SM_{SMAP-L4}$ and SM_{Rec} in each month. SM_{Rec} captures the spatial and temporal variations of $SM_{SMAP-L4}$ well except in the Continental Basin. Although the monthly KGE values in all basins are larger than 0.59 except for the Continental Basin, SM_{Rec} slightly underestimates $SM_{SMAP-L4}$ at the monthly scale in all basins.
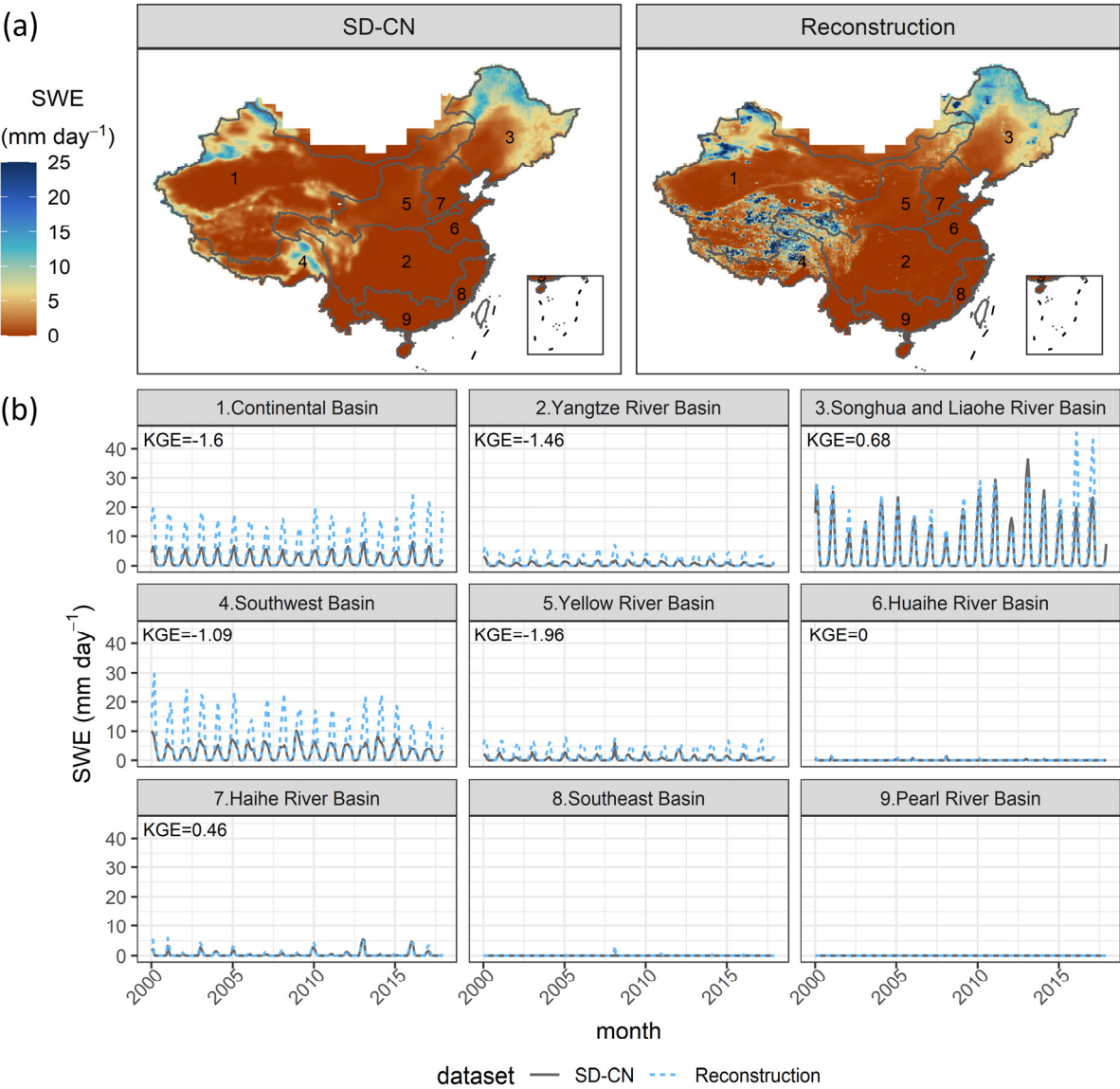
Figure 8. (a) Map of daily average snow water equivalent (SWE) of SD-CN and reconstruction in 2000-2017. (b) Time series of the daily average SWE of SD-CN and reconstruction for nine major river basins in each month of 2000-2017.
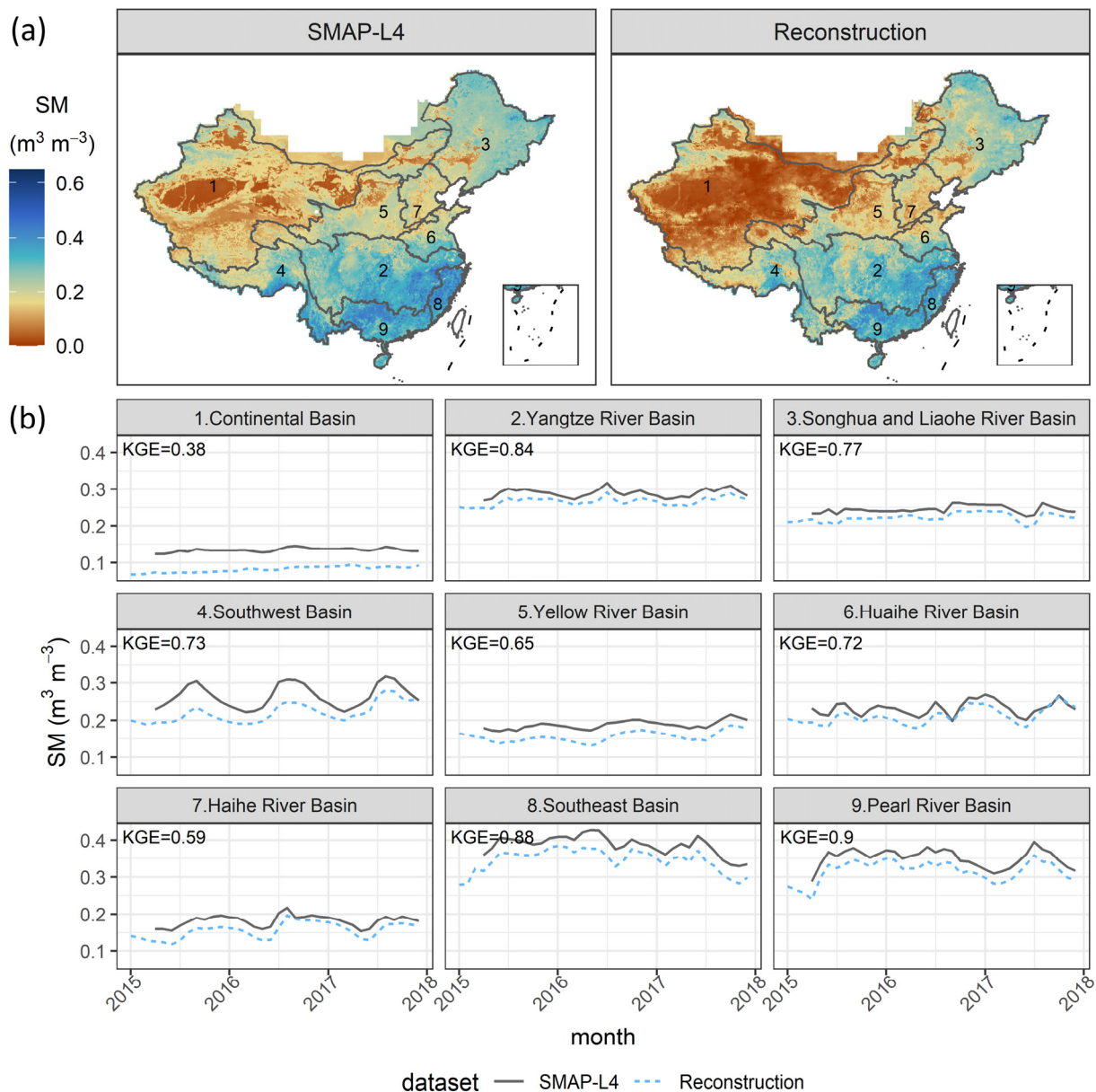
Figure 9. (a) Map of daily average soil moisture (SM) of SMAP-L4 and reconstruction in 2015-2017. (b) Time series of the daily average SM of SMAP-L4 and reconstruction for nine major river basins in each month of 2015-2017.

365

4.3 Limitations of the reconstruction dataset

Uncertainties of the reconstruction dataset come from the quality of the input data and the limitations of the reconstruction models. For precipitation, although the benchmarked dataset CMPA includes satellite information to produce *P* data, it still

has large errors in western China due to the small number of automatic weather stations for local corrections in this area.

370 Another problem of CMPA data is the possible inconsistency between CMPA and its successor, CMPA_1km. Although the main observation sources and the deriving method are similar, the discrepancy between CMPA and CMPA_1km has not been investigated in previous studies. Combining CMPA and CMPA_1km trades consistency for more data samples in machine learning algorithms. In addition, the quality of MSWEP is not consistent over time since the available data sources to be merged are changing in different periods. Furthermore, although the stacking machine learning model can extrapolate, it may

375 have problems in reconstructing extreme P values since the extrapolation relies on a linear regression model, which may fail to capture the complex relationship between the target targeted P and input variables. For snow water equivalent, a unified snow density (0.18 g cm^{-3}) may cause a large bias in estimating SWE in some regions. The coarse resolution of the benchmarked SWE is also a major concern: although the MODIS SCA data add sub-grid information to the 0.25° SD-CN data, we still do not have a benchmarked SWE dataset that is originally 0.1°. Another limitation is the unknown applicability of the

380 HBV model at a national scale. HBV uses a temperature-based snow module without an energy balance component or a glacier module, which may fail in areas with more complex snow processes such as the Tibetan Plateau (Gao et al., 2020). For soil moisture, the benchmarked SMAP-L4 is an assimilated dataset without actual measurements of root zone SM. In addition, PET is calculated without local R_n data. The uncertainty of PET may propagate to SM. Moreover, it is unclear whether HBV is suitable for soil water simulation at a national scale in China.

385 Reconstruction data do not have better accuracy than the satellite-based benchmark data we used. Instead, reconstruction aims to extend the state-of-the-art satellite-based data of P, SM, and SWE to the 1980s in China. Therefore, the value of the reconstruction data is to support hydrological studies focusing on a longer time span (e.g., 30 years) rather than recent years.

5 Conclusions

We created a long-term (1981-2017) 0.1° daily dataset of total precipitation (P), liquid rainfall (Rain), snowfall (Snow), snow

390 water equivalent (SWE), snowmelt (Melt), and soil moisture (SM) in China by reconstructing high-resolution satellite-based data. P was reconstructed by predicting CMPA data from CGDPA and MSWEP data using a stacking machine learning model. Other variables were simulated by the HBV model with SWE calibrated by SD-CN, SCA calibrated by MOD10C1/MYD10C1, and SM calibrated by SMAP-L4. Evaluations of the reconstruction data are as follows.

- Benchmarked by CMPA at a national scale, the median POD and FAR of the reconstructed P are 0.87 and 0.19 respectively

395 for rain/no rain classification, and the median KGE and NRMSE of the reconstructed P are 0.68 and 0.63 respectively for P regression in rainy days. The reconstructed P improves the CGDPA and MSWEP data, whose median KGEs are 0.51 and 0.53. The median KGEs are smaller than 0.43 in the Continental Basin and the Southwest Basin and larger than 0.76 in other major basins. At the monthly scale, all basins have KGE values larger than 0.91 except for the Continental Basin and the Songhua and Liaohe River Basin, where the benchmarked precipitation data in cold seasons are not reliable.

- Benchmarked by SD-CN and MOD10C1/MYD10C1 at a national scale, the median KGE of the reconstructed SWE and the median BACC of the reconstructed SCA are -0.31 and 0.65 respectively. The reconstructed SWE performs the best in the Songhua and Liaohe Basin with KGE=0.55 but performs the worst in the Continental Basin where the median KGE is -2.41. At the monthly scale, the reconstructed SWE captures the monthly variability of ~~observed~~ the SWE derived from SD-CN in all basins. However, the reconstructed SWE only reproduces SWE magnitudes accurately in the Songhua and Liaohe Basin (monthly KGE=0.68) and the Haihe Basin (monthly KGE=0.46) but overestimates the SWE magnitudes in other basins.

- Benchmarked by SMAP-L4 at a national scale, the median KGE of the reconstructed SM is 0.61. SM_{Rec} performs well in southern basins, e.g., the Yangtze River Basin, the Huaihe River Basin, the Southeast Basin, and the Pearl River Basin, where the values of median KGE_{SM} are at least 0.76. SM_{Rec} performs the worst in the Continental Basin where the median KGE_{SM}=0.3. At the monthly scale, the KGE values in all basins are larger than 0.59 except for the Continental Basin.

This study is the first attempt to produce a long-term (at least 30 years) $0.1°$ daily dataset of P, SM, and SWE that combines high-accuracy local information and high-resolution satellite-based data via reconstruction. This dataset is especially suitable for exploring the relationship between riverine streamflow and hydrological drivers since the P, SM, and SWE are produced independently from streamflow data. Future improvements include extending the temporal length of the dataset and formulating a model strategy that handles the spatial variability of the hydrological processes at a national scale.

Code availability

The source codes for model training, model calibration, and data reconstruction are available at https://github.com/YANGOnion/Hydrological-Reconstruction-China.

Data availability

The reconstruction datasets of total precipitation, rainfall, snowfall, snow water equivalent, snowmelt, and soil moisture are freely available at https://doi.org/10.5281/zenodo.5811099 (Yang et al., 2021).

Acknowledgements

We thank the China Meteorological Administration for providing national precipitation data (CGDPA, CMPA, and CMPA_1km) and air temperature data from meteorological stations.

Author contribution

WY and HY conceptualized the study. WY developed the methodology, performed the analysis and wrote the original draft of manuscript. All other authors contributed to review and revise the manuscript. HY, QH, and DY helped in the data collection. HY and DY were responsible for funding acquisition.

430 ## Competing interests

The authors declare that they have no conflict of interest.

Financial support

This research was supported by the China National Key R&D Program (grant no. 2021YFC3000202), the National Natural Science Foundation of China (grant no. 51979140, 42041004) and the State Key Laboratory of Hydro Science and Hydraulic 435 Engineering of China (grant no. 2021-KY-04) .

References

Abelen, S., Seitz, F., Abarca-del-Rio, R., and Guntner, A.: Droughts and Floods in the La Plata Basin in Soil Moisture Data and GRACE, Remote Sens-Basel, 7, 7324-7349, 10.3390/rs70607324, 2015.

Beck, H. E., Pan, M., Miralles, D. G., Reichle, R. H., Dorigo, W. A., Hahn, S., ... & Wood, E. F.: Evaluation of 18 satellite-
440 and model-based soil moisture products using in situ measurements from 826 sensors, Hydrol. Earth Syst. Sci., 25(1), 17-40, 10.5194/hess-25-17-2021, 2021.

Beck, H. E., Pan, M., Lin, P., Seibert, J., van Dijk, A. I., & Wood, E. F.: Global fully distributed parameter regionalization based on observed streamflow from 4,229 headwater catchments, J Geophys Res-Atmos, 125(17), 10.1029/2019jd031485, 2020.

445 Beck, H. E., Wood, E. F., Pan, M., Fisher, C. K., Miralles, D. G., van Dijk, A. I. J. M., McVicar, T. R., and Adler, R. F.: MSWEP V2 Global 3-Hourly 0.1 degrees Precipitation: Methodology and Quantitative Assessment, B Am Meteorol Soc, 100, 473-502, 10.1175/Bams-D-17-0138.1, 2019.

Bergström, S.: The HBV model – its structure and applications, SMHI Reports RH 4, Swedish Meteorological and Hydrological Institute (SMHI), Norrköping, Sweden, 1992.

450 Bloeschl, G., Hall, J., Viglione, A., Perdigao, R. A. P., Parajka, J., Merz, B., Lun, D., Arheimer, B., Aronica, G. T., Bilibashi, A., Bohac, M., Bonacci, O., Borga, M., Canjevac, I., Castellarin, A., Chirico, G. B., Claps, P., Frolova, N., Ganora, D., Gorbachova, L., Gul, A., Hannaford, J., Harrigan, S., Kireeva, M., Kiss, A., Kjeldsen, T. R., Kohnova, S., Koskela, J. J., Ledvinka, O., Macdonald, N., Mavrova-Guirguinova, M., Mediero, L., Merz, R., Molnar, P., Montanari, A., Murphy, C.,

Osuch, M., Ovcharuk, V., Radevski, I., Salinas, J. L., Sauquet, E., Sraj, M., Szolgay, J., Volpi, E., Wilson, D., Zaimi, K.,
455 and Zivkovic, N.: Changing climate both increases and decreases European river floods, Nature, 573, 108-+,
10.1038/s41586-019-1495-6, 2019.

Breiman, L.: Random forests, Mach Learn, 45, 5-32, Doi 10.1023/A:1010933404324, 2001.

Che, T. and Dai, L.: Long-term series of daily snow depth dataset in China (1979-2020). National Tibetan Plateau Data Center,
10.11888/Geogra.tpdc.270194, 2015.

460 Dorigo, W., Wagner, W., Albergel, C., Albrecht, F., Balsamo, G., Brocca, L., Chung, D., Ertl, M., Forkel, M., Gruber, A.,
Haas, E., Hamer, P. D., Hirschi, M., Ikonen, J., de Jeu, R., Kidd, R., Lahoz, W., Liu, Y. Y., Miralles, D., Mistelbauer, T.,
Nicolai-Shaw, N., Parinussa, R., Pratola, C., Reimer, C., van der Schalie, R., Seneviratne, S. I., Smolander, T., and
Lecomte, P.: ESA CCI Soil Moisture for improved Earth system understanding: State-of-the art and future directions,
Remote Sens Environ, 203, 185-215, 10.1016/j.rse.2017.07.001, 2017.

465 Foresee, F. D. and Hagan, M. T.: Gauss-Newton approximation to Bayesian learning, in: Proceedings of international
conference on neural networks, IEEE, Houston, TX, USA, June 1997, 3, 1930-1935, 1997.

Gao, H. K., Dong, J. Z., Chen, X., Cai, H. Y., Liu, Z. Y., Jin, Z. H., Mao, D. H., Yang, Z. J., and Duan, Z.: Stepwise modeling
and the importance of internal variables validation to test model realism in a data scarce glacier basin, J Hydrol, 591,
ARTN 125457 10.1016/j.jhydrol.2020.125457, 2020.

470 Hall, D. K. and Riggs, G. A.: MODIS/Aqua Snow Cover Daily L3 Global 0.05Deg CMG, Version 61, NASA National Snow
and Ice Data Center Distributed Active Archive Center, Boulder, Colorado USA, 10.5067/MODIS/MYD10C1.061,
2021a.

Hall, D. K. and Riggs, G. A.: MODIS/Terra Snow Cover Daily L3 Global 0.05Deg CMG, Version 61, NASA National Snow
and Ice Data Center Distributed Active Archive Center, Boulder, Colorado USA, doi: 10.5067/MODIS/MOD10C1.061,
475 2021b.

Hall, D. K., Riggs, G. A., Salomonson, V. V., DiGirolamo, N. E., and Bayr, K. J.: MODIS snow-cover products, Remote Sens
Environ, 83, 181-194, Pii S0034-4257(02)00095-0 Doi 10.1016/S0034-4257(02)00095-0, 2002.

He, J., Yang, K., Tang, W. J., Lu, H., Qin, J., Chen, Y. Y., and Li, X.: The first high-resolution meteorological forcing dataset
for land process studies over China, Sci Data, 7, 10.1038/s41597-020-0369-y, 2020.

480 Joyce, R. J., Janowiak, J. E., Arkin, P. A., and Xie, P. P.: CMORPH: A method that produces global precipitation estimates
from passive microwave and infrared data at high spatial and temporal resolution, J Hydrometeorol, 5, 487-503, Doi
10.1175/1525-7541(2004)005<0487:Camtpg>2.0.Co;2, 2004.

Li, D. Y., Lettenmaier, D. P., Margulis, S. A., and Andreadis, K.: The Role of Rain-on-Snow in Flooding Over the
Conterminous United States, Water Resour Res, 55, 8492-8513, 10.1029/2019wr024950, 2019.

485 Liang, S. L., Cheng, J., Jia, K., Jiang, B., Liu, Q., Xiao, Z. Q., Yao, Y. J., Yuan, W. P., Zhang, X. T., Zhao, X., and Zhou, J.:
The Global Land Surface Satellite (GLASS) Product Suite, B Am Meteorol Soc, 102, E323-E337, 10.1175/Bams-D-18-
0341.1, 2021.

Luojus, K., Pulliainen, J., Takala, M., Lemmetyinen, J., Mortimer, C., Derksen, C., Mudryk, L., Moisander, M., Hiltunen, M., Smolander, T., Ikonen, J., Cohen, J., Salminen, M., Norberg, J., Veijola, K., and Venalainen, P.: GlobSnow v3.0 Northern Hemisphere snow water equivalent dataset, Sci Data, 8, ARTN 163 10.1038/s41597-021-00939-2, 2021.

Mao, G. Q., and Liu, J. G.: WAYS v1: a hydrological model for root zone water storage simulation on a global scale, Geosci Model Dev, 12, 5267-5289, 10.5194/gmd-12-5267-2019, 2019.

Miao, Y., and Wang, A. H.: A daily 0.25 degrees x 0.25 degrees hydrologically based land surface flux dataset for conterminous China, 1961-2017, J Hydrol, 590, ARTN 125413 10.1016/j.jhydrol.2020.125413, 2020.

Munoz-Sabater, J., Dutra, E., Agusti-Panareda, A., Albergel, C., Arduini, G., Balsamo, G., Boussetta, S., Choulga, M., Harrigan, S., Hersbach, H., Martens, B., Miralles, D. G., Piles, M., Rodriguez-Fernandez, N. J., Zsoter, E., Buontempo, C., and Thepaut, J. N.: ERA5-Land: a state-of-the-art global reanalysis dataset for land applications, Earth Syst Sci Data, 13, 4349-4383, 10.5194/essd-13-4349-2021, 2021.

Myers, D. E.: Matrix Formulation of Co-Kriging, J Int Ass Math Geol, 14, 249-257, Doi 10.1007/Bf01032887, 1982.

Parajka, J., Merz, R., and Bloschl, G.: Uncertainty and multiple objective calibration in regional water balance modelling: case study in 320 Austrian catchments, Hydrol Process, 21, 435-446, 10.1002/hyp.6253, 2007.

Priestley, C. H. B., and Taylor, R. J.: Assessment of Surface Heat-Flux and Evaporation Using Large-Scale Parameters, Mon Weather Rev, 100, 81-+, Doi 10.1175/1520-0493(1972)100<0081:Otaosh>2.3.Co;2, 1972.

Qi, W., Feng, L., Yang, H., and Liu, J. G.: Spring and summer potential flood risk in Northeast China, J Hydrol-Reg Stud, 38, ARTN 100951 10.1016/j.ejrh.2021.100951, 2021.

Reager, J. T., Thomas, B. F., and Famiglietti, J. S.: River basin flood potential inferred using GRACE gravity observations at several months lead time, Nat Geosci, 7, 589-593, 10.1038/Ngeo2203, 2014.

Reichle, R. H., Liu, Q., Koster, R. D., Crow, W., De Lannoy, G. J. M., Kimball, J. S., Ardizzone, J. V., Bosch, D., Colliander, A., Cosh, M., Kolassa, J., Mahanama, S. P., Prueger, J., Starks, P., and Walker, J. P.: Version 4 of the SMAP Level-4 Soil Moisture Algorithm and Data Product, J Adv Model Earth Sy, 11, 3106-3130, 10.1029/2019ms001729, 2019.

Rodell, M., Houser, P. R., Jambor, U., Gottschalck, J., Mitchell, K., Meng, C. J., Arsenault, K., Cosgrove, B., Radakovich, J., Bosilovich, M., Entin, J. K., Walker, J. P., Lohmann, D., and Toll, D.: The global land data assimilation system, B Am Meteorol Soc, 85, 381-+, 10.1175/Bams-85-3-381, 2004.

Seibert, J., and Bergström, S.: A retrospective on hydrological catchment modelling based on half a century with the HBV model, Hydrol. Earth Syst. Sci., 26(5), 1371-1388, 10.5194/hess-26-1371-2022, 2022

Sharma, A., Wasko, C., and Lettenmaier, D. P.: If Precipitation Extremes Are Increasing, Why Aren't Floods?, Water Resour Res, 54, 8545-8551, 10.1029/2018wr023749, 2018.

Shen, Y., Hong, Z., Pan, Y., Yu, J. J., and Maguire, L.: China's 1 km Merged Gauge, Radar and Satellite Experimental Precipitation Dataset, Remote Sens-Basel, 10, ARTN 264 10.3390/rs10020264, 2018.

Shen, Y., and Xiong, A. Y.: Validation and comparison of a new gauge-based precipitation analysis over mainland China, Int J Climatol, 36, 252-265, 10.1002/joc.4341, 2016.

Shen, Y., Zhao, P., Pan, Y., and Yu, J. J.: A high spatiotemporal gauge-satellite merged precipitation analysis over China, J Geophys Res-Atmos, 119, 3063-3075, 10.1002/2013jd020686, 2014.

Stein, L., Clark, M. P., Knoben, W. J. M., Pianosi, F., and Woods, R. A.: How Do Climate and Catchment Attributes Influence Flood Generating Processes? A Large-Sample Study for 671 Catchments Across the Contiguous USA, Water Resour Res, 57, ARTN e2020WR028300 10.1029/2020WR028300, 2021.

Tarasova, L., Basso, S., Wendi, D., Viglione, A., Kumar, R., and Merz, R.: A Process-Based Framework to Characterize and Classify Runoff Events: The Event Typology of Germany, Water Resour Res, 56, ARTN e2019WR026951 10.1029/2019WR026951, 2020.

Van Steenbergen, N., and Willems, P.: Increasing river flood preparedness by real-time warning based on wetness state conditions, J Hydrol, 489, 227-237, 10.1016/j.jhydrol.2013.03.015, 2013.

Wolpert, D. H.: Stacked Generalization, Neural Networks, 5, 241-259, Doi 10.1016/S0893-6080(05)80023-1, 1992.

Yamazaki, D., Ikeshima, D., Sosa, J., Bates, P. D., Allen, G. H., and Pavelsky, T. M.: MERIT Hydro: A High-Resolution Global Hydrography Map Based on Latest Topography Dataset, Water Resour Res, 55, 5053-5073, 10.1029/2019wr024873, 2019.

Yang, J. W., Jiang, L. M., Lemmetyinen, J., Luojus, K., Takala, M., Wu, S. L., and Pan, J. M.: Validation of remotely sensed estimates of snow water equivalent using multiple reference datasets from the middle and high latitudes of China, J Hydrol, 590, ARTN 125499 10.1016/j.jhydrol.2020.125499, 2020.

Yang, J. W., Jiang, L. M., Wu, S. L., Wang, G. X., Wang, J., and Liu, X. J.: Development of a Snow Depth Estimation Algorithm over China for the FY-3D/MWRI, Remote Sens-Basel, 11, ARTN 977 10.3390/rs11080977, 2019.

Yang, W. C., Yang, H. B., and Yang, D. W.: Classifying floods by quantifying driver contributions in the Eastern Monsoon Region of China, J Hydrol, 585, ARTN 124767 10.1016/j.jhydrol.2020.124767, 2020.

Yang W. C., Yang, H. B., Li, C. M., Wang, T. H., Liu, Z. W., Hu, Q. F., and Yang, D. W.: Long-term reconstruction of satellite-based precipitation, soil moisture, and snow water equivalent in China (1.0), Zenodo, https://doi.org/10.5281/zenodo.5811099, 2021.

Zhang, X. J., Tang, Q. H., Pan, M., and Tang, Y.: A Long-Term Land Surface Hydrologic Fluxes and States Dataset for China, J Hydrometeorol, 15, 2067-2084, 10.1175/Jhm-D-13-0170.1, 2014.

Zhu, B. W., Xie, X. H., Lu, C. Y., Lei, T. J., Wang, Y. B., Jia, K., and Yao, Y. J.: Extensive Evaluation of a Continental-Scale High-Resolution Hydrological Model Using Remote Sensing and Ground-Based Observations, Remote Sens-Basel, 13, ARTN 1247 10.3390/rs13071247, 2021.